Electronic structure and lattice dynamics in kesterite-type $Cu_2ZnSnSe_4$ from first-principles calculations

Narjes Beigom Mortazavi Amiri and Andrei Postnikov
LPMD, Institute Jean Barriol, Université Paul Verlaine–Metz, 1 Bd Arago, F-57078 Metz, France
(Received 10 April 2010; revised manuscript received 31 August 2010; published 8 November 2010)

Electronic band structure, densities of states, and the details of chemical bonding in $Cu_2ZnSnSe_4$, a compound used in photovoltaic applications and structurally close to chalcopyrite, has been studied using the SIESTA method within the local-density approximation of the density-functional theory. Calculated zone-center phonons for $Cu_2ZnSnSe_4$ in kesterite and stannite phases reveal a similarity to those in structurally close $CuInSe_2$, with some additional modes which must become observable due to the reduced crystal symmetry. The prediction that the highest TO vibration mode has predominantly Zn contribution is consistent with a strong Zn concentration dependence of this particular mode earlier observed in (Zn,Cd)-mixed kesterite systems. A detailed comparison of calculated vibration spectra for kesterite and stannite phases helps to identify the features which could be useful for distinguishing these two structures in practice.

DOI: 10.1103/PhysRevB.82.205204 PACS number(s): 71.20.Nr, 88.40.jn, 63.20.dk

I. INTRODUCTION

Chalcopyrite-type $CuInSe_2$ (CIS) has a long-established reputation as one of the most promising materials for thin film solar cell applications. As a need for searching substitutes for indium, a relatively rare and potentially very expensive component, was gradually recognized, $Cu_2ZnSnSe_4$ (CZTSe) emerged as a possible candidate, a homolog to another new photovoltaic material, Cu_2ZnSnS_4 (CZTS).[1] Thin films of these compounds have suitable optical band-gap energy and large optical absorption coefficient of $\sim 10^4$ cm^{-1}—see Refs. 2–7.

These new quaternary materials exist in various modifications, namely, stannite (ST) and kesterite (KS);[8,9] moreover the third structure, primitive mixed CuAu-type, permits to satisfy the chemically plausible coordinations of different cations around the anion. Suggestions have been made that the experimentally reported stannite structure is probably in fact a partially distorted kesterite.[10]

Important for prospective materials in photovoltaics are their efficiency to absorb in the spectral range of maximum intensity for the natural light, along with the stability of their properties against the formation of irradiation-induced structural defects. The reported band gap for $Cu_2ZnSnSe_4$ (Refs. 11–13) is between 1.4 and 1.65 eV.[9,14] This material could be an ideal thin-film solar cell absorber due to its band gap and, moreover, its composition from nontoxic and naturally abundant elements.[1,9,15,16]

The efficiencies of beyond 6% have been achieved so far for these new quaternatry compounds,[16] that is somehow inferior to those of CIS but still rewarding in view of low cost. Up to now, very little effort has been put into understanding of basic properties of these new materials. Not even for such fundamental parameter as the band gap was the agreement reached: the values reported (for CZTS) vary between 1.4 eV (Ref. 4) and 1.6 eV.[3] The scattering of values was assumed to be due to uncontrolled composition variations.[15]

The structural and electronic properties of CZTSe has been investigated by Chen *et al.*[9] using first-principles total energy and band structure calculations within the density functional formalism as implemented in the VASP code. The authors also calculated the partial and total density of states (DOS) of CZTS in the KS and ST structures.[9] A series of binary (II-VI), ternary (I-III-VI_2), and quaternary (I_2-II-IV-VI_4 and I-III-II_2-VI_4) chalcogenides has been studied by Chen and Gong.[10] They investigated the properties (crystal and electronic structures) of these materials from the cation substitution perspective, in order to elucidate the underlying chemical trends. First-principles investigations based on the generalized gradient and hybrid functionals have been carried out by Paier *et al.*[1] for CZTS, concentrating on its ground-state structure, electronic structure, and optical properties. The electronic structure of stannite-type CZTSe was studied by first-principles calculations by Nakamura *et al.*[8] Raulot *et al.* reported *ab initio* results on a number of potential indium- and gallium-free quaternary compounds,[17] including CZTSe, with the accent set at the evaluation of band gaps and the formation energies of intrinsic defects.

First-principles calculations of CIS and related chalcopyrite-type compounds are also quite numerous; we only cite Refs. 18 and 19 as examples of more or less systematic studies. In this paper, we investigate structural and electronic properties of kesterite and stannite-type $Cu_2ZnSnSe_4$ from first principles, using a density-functional theory (DFT) method, with a special interest for zone-center phonons. While the electronic structure of both phases was studied in comparison earlier, the aspect of lattice vibrations, to our knowledge, has not been addressed. We'll see that the overall similarity of spectra of kesterite and stannite is accompanied by differences in nature and frequency of some modes that might prove helpful for structure characterization of samples. Moreover it is an interesting example of how short-range coupling patterns, within a material of a given composition, reveal themselves in the properties of zone-center vibrations. Another comparison is done to calculated phonons in chalcopyrite-type CIS. Here, the differences arise due to the replacement of indium by (Zn,Sn) atoms. As phonon frequencies provide a sensitive probe of elastic constraints within the material, we hope this study to be useful

for subsequent characterization of doped and otherwise nonperfect crystals.

II. STRUCTURE CONSIDERATIONS AND DETAILS OF CALCULATION

The underlying structure of the quaternary compound in question is traditional semiconductor zinc blende; the anion component (unique and, in the following, always selenium) retains its position in the II-VI (say, ZnSe) basic unit. Splitting cation sites in two groups (say Zn into Cu+In) and maintaining a corresponding ordering within each cation plane makes the (tetragonal body centered, with $c \approx 2a$) chalcopyrite, (I,III)-VI. Its space group is $I\bar{4}2d$ (Nr 122) (Ref. 20) with cations in (a) and (b) sites and anions in (d); in total eight atoms per primitive cell. The kesterite structure is a further symmetry lowering from chalcopyrite, albeit within the same tetragonal system, now splitting the cation (III) site (i.e., indium) into II (Zn) and IV (Sn), according to the $I\bar{4}$ (Nr 82) space group. Cu occupies two (now inequivalent) positions (a) and (c), Sn is in (b) and Zn in (d) while Se occupies the (g) positions.[21] Each cation is in a (differently) slightly distorted tetrahedral Se_4 environment whereas the Se anions are slightly displaced from the center of identical and perfect (neglecting the slight $c \neq 2a$ disparity) Cu_2SnZn tetrahedra.

The structure optimization involves the a, c adjustment along with the x internal coordinate for cations. In the calculation by the SIESTA method[22–24] applied here, this is done simultaneously on the basis of available forces and stress tensor elements. SIESTA uses norm-conserving pseudopotentials and strictly confined numerical atom-centered basis functions. Our pseudopotentials were generated with the following valence configurations and pseudoization radii (in Bohr, set in parentheses after the number of valence electrons in each l channel):

$$\text{Cu } 4s^1(2.77)4p^0(2.39)3d^{10}(2.16)4f^0(2.16);$$

$$\text{Sn } 5s^2(2.43)5p^2(2.49)5d^0(2.82)4f^0(2.82);$$

$$\text{Zn } 4s^2(2.43)4p^0(2.37)3d^{10}(2.09)4f^0(2.82);$$

$$\text{Se } 4s^2(1.94)4p^4(2.14)4d^0(1.94)4f^0(2.49).$$

The basis functions were constructed along the standard procedure in SIESTA, as Kohn-Sham orbitals of a confined pseudoatom, to the "double-ζ with polarization orbitals" quality—see Refs. 25 and 26 on the details of basis generation and optimization. The "MeshCutoff" parameter of 360 Ry was taken, that corresponds to 60 divisions along the a lattice parameter in the real-space mesh used for a solution of the Poisson equation with a general-shape residual density in SIESTA. The $3\times3\times3$ k mesh (18 inequivalent k points) was checked to be sufficient to yield sufficiently converged forces. The local-density approximation (LDA) was used throughout.

Phonon frequencies and eigenvectors have been calculated by a finite-displacement method, consecutively allowing small (0.04 Bohr) deviations of each atom from its equilibrium position along positive and negative Cartesian directions, accumulating the force constants calculated from forces by finite differences, and diagonalizing dynamical matrix without taking any symmetry constraints into account. The subsequent identification of phonon modes by symmetry may follow from the analysis of their eigenvectors. Only zone-center TO modes have been thus calculated.

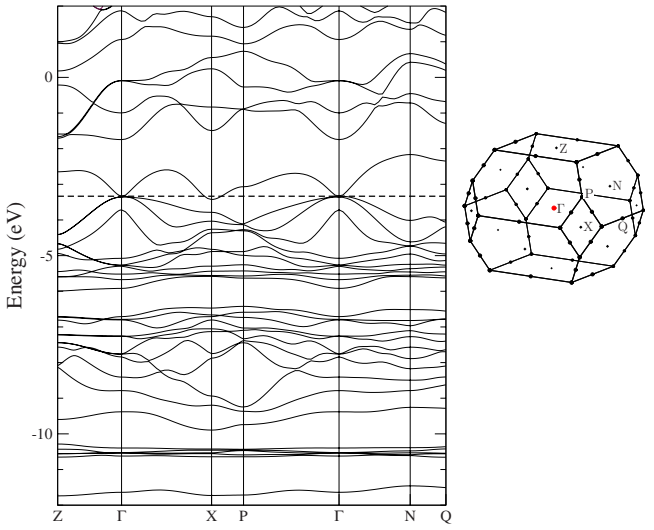

FIG. 1. (Color online) Band structure of $Cu_2ZnSnSe_4$ kesterite as calculated in the LDA by SIESTA.

In our discussion, we make reference to similar calculations for $CuInSe_2$ chalcopyrite, done earlier by one of us[27] by the same method and now repeated with the choice of pseudopotentials and the basis set as discussed above, notably the In pseudopotential generated for the atomic configuration In $5s^2(2.54)5p^1(2.61)5d^0(2.88)4f^0(2.42)$.

III. BAND STRUCTURE AND CHEMICAL BONDING

As was outlined in the Introduction, a number of previous DFT calculations exist, either for CZTS in different modifications[1,28] or for CZTSe stannite,[8] which yield largely similar features of their electronic structures. Therefore global features of electronic structures in these materials are roughly known; however, the differences between sulphide and selenide seem to be not quite trivial, and the differences between stannite and kesterite not negligible, that justifies our present study.

Our band structure is shown in Fig. 1, and partial DOS—in Fig. 2. The relaxed LDA lattice parameters are $a=5.639$ Å, $c=11.234$ Å—to be compared with experimental (thin film) $a=5.68$, $c=11.36$ Å,[14] or (without specifying the exact phase) $a=5.693$, $c=11.33$ Å of Ref. 29. The deviation from ideal cubic relation is very small, as indeed known for kesterite.[9] This previous generalized gradient approximation (GGA) calculation by Chen *et al.*[9] gave a slightly overestimated lattice parameter. The internal coordinates of Se atoms, the only ones with positions not fixed by symmetry, are $(x,y,z)=(0.772,0.236,0.132)$. Comparing this with "ideal" values $(\frac{3}{4},\frac{1}{4},\frac{1}{8})$ shows that the displacement

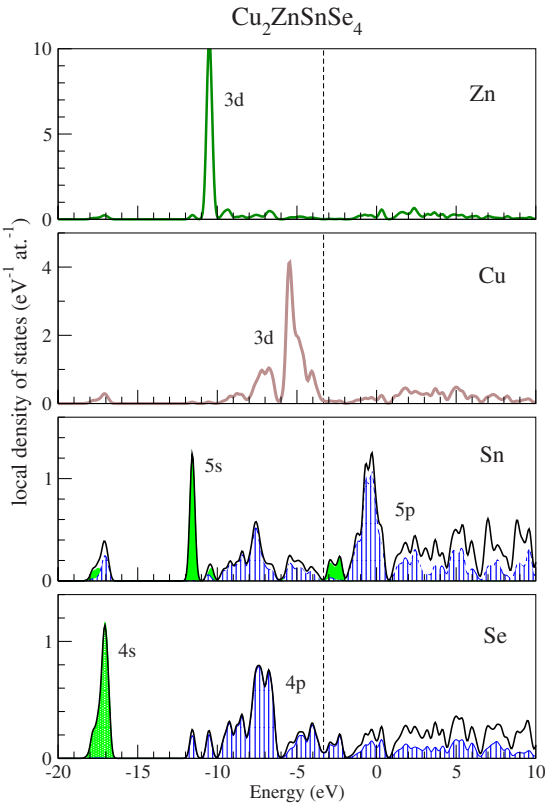

FIG. 2. (Color online) Partial densities of states (normalized per atom) in $Cu_2ZnSnSe_4$ kesterite, broadened with the width parameter of 0.2 eV.

of Se from the center of its tetrahedron is not negligible: the bond lengths to Cu, Zn, and Sn are 2.37, 2.42, and 2.60 Å, correspondingly. They can be compared with single crystal x-ray diffraction data of Olekseyuk *et al.*[30] (Cu–Se 2.436 Å, Zn–Se 2.426 Å, Sn–Se 2.539 Å, which relate, however, to the stannite structure).

The system of upper valence states above the Se 4*s* (which is shown in our DOS plot but not in the band structure) splits into four well separated groups: the predominantly Sn 5*s* one at ~8 eV below the valence band top (hence at ~−11.5 eV in our absolute energy scale); the Zn 3*d* band ~1 eV higher (we will also see a non-negligible contribution of Zn 3*d* throughout upper-lying states), and two bunches of bands having the Cu 3*d*−Se 4*p* nature. The presence of Sn 5*p* states in the energy region (−10:−3) eV, implied by the DOS plot, is spurious and reveals an expansion over other atoms' states on the Sn-centered basis functions. The genuine Sn 5*p* states will start in the conduction band only. Among the two Cu 3*d*−Se 4*p* related subbands, the lower one seems to be of bonding character, involving predominantly the e_g symmetry at the Cu site; the upper bunch involves mostly t_{2g} states at the Cu site, which do not form bonding combinations with Se 4*p*. Such intuitive characterization by symmetry and bonding type is supported by Fig. 3 which depicts the energy-dependent spatial charge density, $\rho(E,\mathbf{r})$, integrated over the corresponding energy intervals, namely, (−10:−6) and (−6:−3) eV in our absolute energy scale, in two ways. The main plot explicitly traces $\rho(E_1{:}E_2,\mathbf{r})$ along the bonds from one atom to another

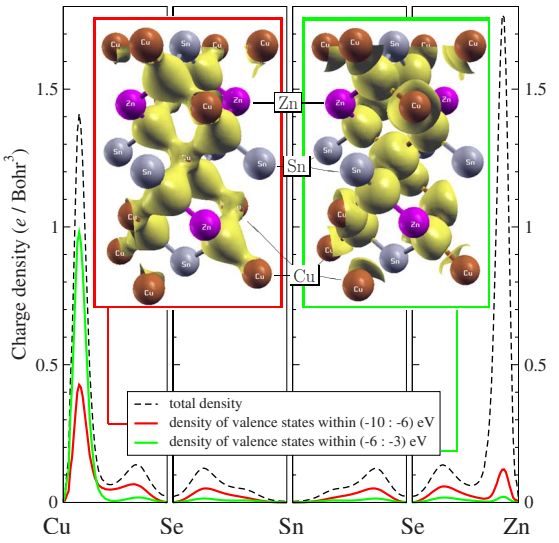

FIG. 3. (Color online) Charge density profile (of pseudovalence states) along the lines connecting different atoms, total (dashed line) and within two energy intervals, (−10:−6) eV (red line) and (−6:−3) eV (green line). In the inset, the isosurfaces of two integrated densities are shown within boxes of the corresponding color. See text for details.

whereas the inset shows isosurfaces at a conveniently chosen value. Note a relative disappearance of the (−6:−3) eV charge density some place along the bond, a "cubiclike" character of the corresponding isosurface around the Cu site (see right inset in Fig. 3)—a manifestation of its t_{2g}-like nature, and an absence of charge density around the Sn site.

The nature of chemical bonding can be further revealed by an analysis of Kohn-Sham eigenfunctions. The contour and isosurface plots for some of them at $\mathbf{k}=0$, immediately below/above the band gap, are shown in Fig. 4. Among 31 occupied bands/$\mathbf{k}=0$ states, the upper two are degenerate, and have roughly the same composition and just different spatial orientation of Cu/Zn t_{2g} vs. Se 4*p* lobes (always in antibonding setting) as their third partner in the lowest unoccupied band. Turning to the "next-from-the gap" eigenfunctions, we note that the Nr 29 (having maximum at Γ 0.36 eV below the valence band top) is nonbonding in what regards the Se 4*p*−Cu/Zn e_g interaction and antibonding with respect to the Se 4*p*−Sn 5*s* coupling. The unoccupied band Nr 33 hosts the Sn 5*p* states, which knit their banana-shaped lobes to the 4*p* of neighboring Se in a nice complicated pattern. The states further up in the conduction band also have large contribution of Sn 5*p*, arranging it in a complex manner with Se 4*p*.

The above analysis of chemical bonding closely follows that of Paier *et al.*[1] for the sulfur-based kesterite, although slightly different properties were inspected there, and the localization of electronic states on S atoms seems stronger than on Se in our case.

We found a disappearingly small gap at Γ (0.029 eV), consistently with the results of other straight LDA or GGA calculations (e.g., 17 μeV in Ref. 8 pour CZTSe-stannite) and at variance with the experimental gap value of 1.44 eV.[29] In fact, we found a small negative indirect gap of −0.071 eV, due to a conduction band minimum at *X* (see

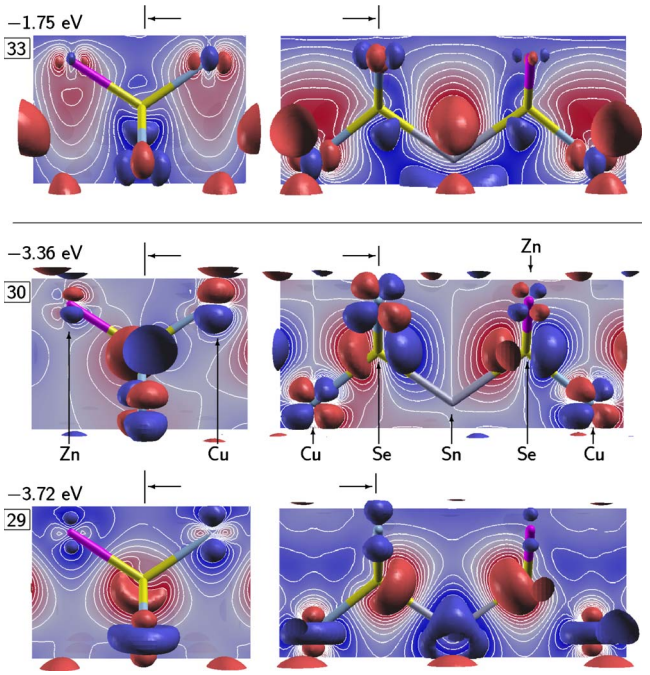

FIG. 4. (Color online) Isosurfaces (at ± 0.05 Å^{-3}) and contours (from 0.05 to −0.05; linear step of 0.01 Å^{-3}; different colors indicate positive/negative values) of selected zone-center Kohn–Sham functions. Band indexes (number of occupied bands: 31) are shown in boxes on the left, beside the corresponding band energies. Left/right plots are views in different cutting planes of the same rectangular prism, chosen to comprise all atom types. The trace of the other cutting plane and the direction of view is shown in the upper part of each counterpart plot.

Fig. 1). Chen *et al.*[9] reported a negative gap of −0.30 eV (which becomes positive on applying a hybride functional), without, however, specifying its nature. Paier *et al.*[1] in their calculation for CZTS kesterite reported a direct gap at Γ.

An analysis of previously done electronic structure calculations hints that the problem of "negative gap," and hence a (wrongly) semimetallic character of our material under study, can be cured by applying a hybride functional but prevails throughout "conventional" LDA or DFT calculations. A too small band gap value would pose problem for an analysis of optical properties that is not our objective here. In what regards lattice dynamics calculations, however, we do not *a priori* expect big error, by force of the following arguments. First, a considerable experience exist for elemental Ge for which DFT calculations fail to find a true band gap but predict its lattice dynamical properties correctly. Second, the lattice dynamical spectra of kesterite and stannite, discussed further, show a fair similarity with the spectrum of chalcopyrite-type CIS, inasmuch this similarity can be expected; yet CIS does not suffer from the negative gap problem.

IV. LATTICE DYNAMICS

It seems instructive to compare the phonon spectra and the structure of vibration modes between kesterite and stannite phases of CZTSe, in order to see a possible effect of different connectivity within the same composition. Moreover, we make reference to the lattice dynamics of chalcopyrite-type $CuInSe_2$, in which the Sn and Zn sites are taken by indium. The phonon modes in the latter compound have been calculated by Łażewski *et al.*[31] and by one of us in Ref. 27. The comparison with Raman spectra demands the knowledge of zone-center vibration frequencies. The latter follow directly from our finite-displacement calculation of phonons in a primitive cell (eight atoms). The subtlety is, however, in a presence of two formula units in the primitive cell of chalcopyrite, which produces some vibration modes involving the movement of identical atoms in counterphase, and hence silent for a detection by Raman spectroscopy. Therefore we represent our calculation results in twofold manner. First, we give a full list of vibration modes, numbered from 4 on (skipping three zero-frequency acoustic modes) through $8\times 3=24$, and provide a brief description of each mode—see Tables I and II. Some degeneracies come about, due to tetragonal symmetry. Moreover, for most modes, at least in what regards the displacement of cations, a neat separation occurs into the "in-plane" (x,y) displacement and the z displacement. The vibration pattern of Se anions is of more general character but often enough the pattern of "along the chain" displacements can be recognized, involving one or another cation sequence. We will see that some of these patterns differ in kesterite and in stannite. Some fancy vibration modes, or those needed for the subsequent discussion, are further on visualized by "snapshots."

The second way to characterize the vibration spectra is by local (atom-resolved) density of modes, projected onto a spatial wave with a given $\mathbf{q}$ in crystal,

$$I_{\aleph}^{\mathbf{q}}(\omega)=\sum_i\left(\sum_{\alpha\in\aleph}\mathbf{A}_{i\alpha}e^{i\mathbf{q}\mathbf{R}_\alpha}\right)^2\delta(\omega-\omega_i),\qquad(1)$$

where α numbers the atoms of a given species $\aleph$, situated at $\mathbf{R}_\alpha$ in the unit cell, i runs over vibration modes, having frequencies ω_i and eigenvectors $\mathbf{A}_{i\alpha}$. $\delta(\omega)$ is an artificially broadening function, for better visibility of a discrete spectrum (the Lorentzian with halfwidth of 5 cm^{-1} in the figure below). This approach helps to extract something like phonon spectral function, e.g., in alloys,[32] and in our case of pure compounds—to enhance vibration patterns with genuine "in-phase" movement of Cu or Se atoms, multiply present in the unit cell. This will suppress the silent modes and enhance those which mostly contribute to the Raman spectra. The true Raman intensities, involving corresponding matrix elements, are not calculated, hence the comparison of spectral intensities attributed to chemically different atoms is not possible.

We address first the results on $CuInSe_2$ chalcopyrite. In Fig. 5, the upper panel depicts the density of $\mathbf{q}=0$ vibration modes, calculated here anew by the SIESTA method with the calculation parameters as specified above, and in comparison with experimental data. In agreement with the results of Ref. 31 (which provide, however, a total phonon density of states), three main groups of lines are visible: the mostly Cu+In ones at about 70 cm^{-1}, an isolated Cu+In-mode at 170 cm^{-1} and a group of lines with complex interplay of Cu,

TABLE I. Calculated zone-center vibration modes in CZTSe-kesterite. The "description" column refers to (Cu,Sn) or (Cu,Zn) (001) planes, e.g., Cu+Sn when the two cations of a given plane vibrate in phase, and, e.g., Cu-Sn when they vibrate in opposite. For degenerate modes (whose numbers in the first column are doubled), a description of only one is given; the second mode can be obtained by a $(x \leftrightarrow y)$-switch. "Silent" in relation to Se vibration means that the latter is fully symmetric over the four Se atoms in the unit cell, not changing the related dipole moment. Asterisks mark modes further shown in the figures.

Mode Nr	Frequency (cm^{-1})	Description
4,5	64	Cu+Sn$\parallel$[110], against Cu+Zn
6	75	all Cu$\parallel$[001]; Zn and Sn$\parallel[00\bar{1}]$; Se in (xy) plane, silent
7,8	81	Cu-Sn$\parallel[\bar{1}10]$; Cu-Zn$\parallel$[110]; two of four Se$\parallel \pm$[001] (*)
9	88	Cu-Sn$\parallel$[001]; Cu-Zn$\parallel[00\bar{1}]$; Se in (xy) plane, silent
10,11	174	Cu-Sn$\parallel$[110]; Cu-Zn$\parallel[\bar{1}10]$; Se silent
12	178	Se-only symmetric (silent) mode
13	187	Cu+Sn$\parallel$[001]; Cu+Zn$\parallel[00\bar{1}]$; Se silent
14	192	Se-only in the (xy) plane; silent
15	203	Se-only; silent
16,17	211	Sn$\parallel$[110]; longitudinal vibration of Se against Sn in the -Sn-Se-Cu-Se-Sn- chains (*)
18	216	All cations Cu, Zn, Sn$\parallel$[001], against Se
19,20	224	Cu+Sn$\parallel$[110]; Cu+Zn$\parallel[1\bar{1}0]$; net Se contribution (*)
21	230	Cu-Sn$\parallel$[001]; Cu+Zn$\parallel$[001]; net Se contribution
22	237	Cu-Zn$\parallel$[001]; Se in (xy) plane
23,24	239	Zn$\parallel[\bar{1}10]$; longitudinal vibration of Se against Zn(+); in the -Cu-Se-Zn-Se-Cu- chains (*)

In, and Se at 200–250 cm^{-1}. One can note a satisfactory agreement with experiment in positioning of peaks, notwithstanding some distortion toward the higher frequencies (the calculation seems to underestimate some experimental frequencies by as much as 8%). It is interesting to study how these modes will be affected as In cations gets substituted by

TABLE II. Similar to Table I, for CZTSe-stannite. The description column refers to (Zn,Sn) or (Cu,Cu) (001) planes in stannite, e.g., Zn+Sn when the two cations of a given plane vibrate in phase, and. e.g., Cu-Cu when they vibrate in opposite. δ as the third coordinate means a noticeable deviation from planarity. Among the modes 21–23, the identification of two genuinely degenerate ones is complicated by an occasional degeneracy with the third one.

Mode Nr	Frequency (cm^{-1})	Description
4,5	60	Zn+Sn$\parallel$[100], against Cu+Cu
6	72	Cu-Cu$\parallel$[001]; Se in (xy) plane, silent
7	79	Zn-Sn$\parallel$[001]; Se almost in (xy) plane, silent
8,9	90	Zn-Sn$\parallel$[010]; Cu-Cu$\parallel$[100]; Se$\parallel \pm$[001], silent (*)
10	175	Se-only symmetric (silent) mode
11,12	180	Zn-Sn$\parallel[11\delta]$; Cu-Cu$\parallel[\bar{1}1\bar{\delta}]$; Se silent
13	180	Zn$\parallel[\bar{1}0\delta]$; Cu$\parallel[01\bar{\delta}]$
14	196	Se-only in the (xy) plane; silent
15	203	Se-only symmetric (silent) mode
16,17	209	Zn+Sn$\parallel$[110], against (half of) Se; longitudinal vibration in the Zn-Se-Sn-Se-Zn chains (*)
18	222	Sn$\parallel$[001], against Se
19,20	226	Cu$\parallel[1\bar{1}0]$, against half of Se; longitudinal vibration in the Cu-Se-Cu-Se-Cu chains (*)
21	232	Zn$\parallel[1\bar{1}0]$; Cu-Cu$\parallel$[001]; Se silent (*)
22	232	Zn$\parallel[1\bar{1}0]$; two Cu$\parallel[\bar{1}00]$ and two $\parallel$[010] (*)
23	232	Zn$\parallel$[110]; Cu roughly opposite; two Se against Zn and two other Se against Cu (*)
24	254	Zn$\parallel$[001]; Se in the opposite $\parallel$ to Zn-Se bonds

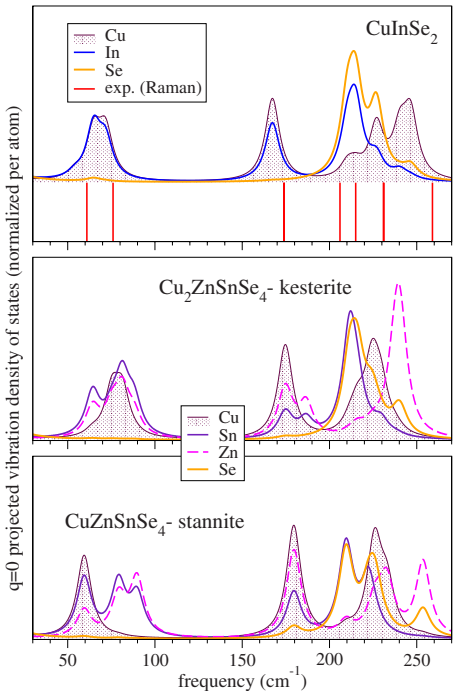

FIG. 5. (Color online) $\mathbf{q}=0$ projected density of vibration modes for different atoms in $Cu_2ZnSnSe_4$-kesterite (middle panel), compared with that of $Cu_2ZnSnSe_4$-stannite (bottom panel) and $CuInSe_2$-chalcopyrite (top panel). The frequencies experimentally detected by Raman scattering for the latter system are indicated by vertical bars.

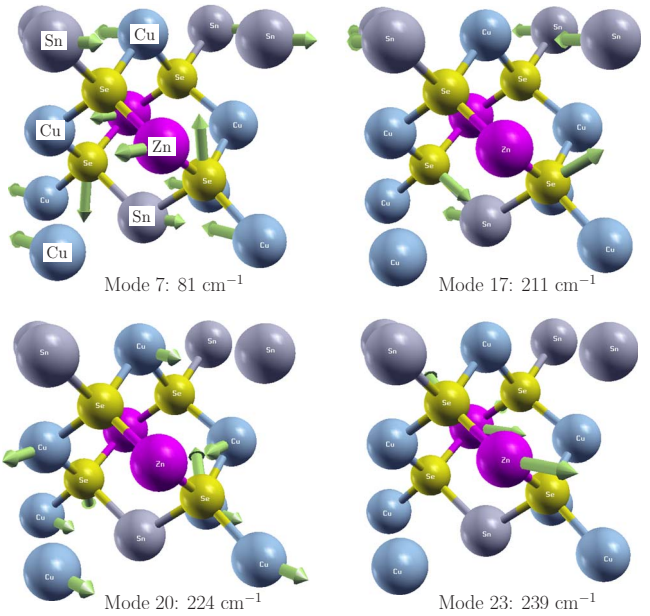

FIG. 6. (Color online) Vibration patterns in selected modes of CZTSe-kesterite. See text for discussion.

Sn and Zn, with corresponding lowering of symmetry, to which end only scarce experimental data exist (see below).

The first impression from looking at the calculated spectrum of kesterite (Fig. 5, middle panel) is that three main groups of lines rest in place, the role of In is taken over by Sn and Zn, without much shift in frequency; the contribution of Se is hardly affected at all. There are, however, noticeable differences: the low-frequency band (between 50 and 100 cm^{-1}) becomes broader and more structured; the Cu contribution is cut at the high-frequency side and "replaced" by a large Zn-related peak.

An inspection of modes shows that these differences are primarily related to changed symmetry properties. Indeed, the low-frequency band, in both chalcopyrite and kesterite, consists of four peaks, degenerate as 2-1-2-1, in the order of increasing frequencies. The Cu contributions over these peaks are roughly the same between chalcopyrite and kesterite; the combined effect of Zn and Sn approximates that of In. The difference between the four peaks is in the relative movement of Cu-containing cation planes. The vibration patterns within some modes are shown in Fig. 6. Two (double degenerate) modes among the discussed four, namely, those at 64 and 81 cm^{-1}, involve the (x,y) planar movement of cations. The difference is that in the 64 cm^{-1} mode, the Cu-Sn plane moves in opposite to the Cu-Zn one whereas in 81 cm^{-1}, roughly all Cu move against both Zn and Sn. Two other low-frequency modes, those at 75 and 88 cm^{-1}, involve the z displacement of the cations; in the first of these modes, all Cu are in opposite movement to both Zn and Sn whereas in the 88 cm^{-1} mode, Cu in the Cu-Sn plane moves along with Zn, and opposite to Cu in the Cu-Zn planes which is in phase with Sn. Due to such criss-cross arrangement, the lowest and the highest modes are Raman-silent in chalcopyrite but must become observable in kesterite, because of the difference between Zn and Sn. The vector sum of Se displacements gives zero in all these four modes, hence the absence of the Se $\mathbf{q}$-projected vibration density throughout the lower spectral part (see Fig. 5), even if relative movement of each Se atom is not small.

Among the "intermediate" modes (those between 150 and 200 cm^{-1}), the softer one involves the (x,y) movement of all atoms and is doubly degenerate. Cu atoms in consecutive planes move toward Zn or toward Sn, respectively, along directions turning by $\pm 90°$ when coming from plane to plane. Hence the in-phase component exists in the movement of Cu taken in total, that results in a strong zone-center peak (at 174 cm^{-1}). The next mode (at 187 cm^{-1}) involves the z displacement of the whole Cu-Sn plane against the Cu-Zn one (like as in the 64 cm^{-1} mode but with different polarization, moreover without a marked Se involvement). Hence it is a silent mode in chalcopyrite, which must become detectable in kesterite.

The upper group of lines starts with the (x,y) planar (hence doubly degenerate) movement of Sn against Se, with only moderate contribution of Cu and Zn. The difference in masses between Sn and In being negligible, the mode frequency (211 cm^{-1}) is the same as in chalcopyrite. The immediately following mode at 216 cm^{-1} is practically a clean z-polarized "zincblende-TO" mode: all cations move in phase against all anions. (We note the closeness of its frequency to the TO mode of binary ZnSe, at 205–207 cm^{-1}); this is the mode with the strongest Se contribution. An interesting mode, absent in chalcopyrite, is that at 230 cm^{-1}: Cu with Zn vibrate in phase along z, against the Sn. In the mode at 237 cm^{-1}, the Cu-Sn planes remain (almost) still whereas

the Cu-Zn ones planes vibrate along z (Cu opposite with Zn); again a behavior not encountered in chalcopyrite. This overlaps with the topmost double degenerate mode (239 cm^{-1}), which involves (x,y) movement of (roughly rigid) Cu-Sn and Cu-Zn planes, at 90° one to another. A remarkable feature of the vibration spectrum of kesterite is the enhancement of the Zn contribution toward the upper end of the spectrum, instead of being evenly distributed over the 200–250 cm^{-1} band, like that of Cu (or, of In in chalcopyrite).

Our theoretical prediction gets support from the only experimental measurement we could find on the CZTSe system,[33] studied as powder and without specifying its structure type. The Raman spectra of $Cu_2Zn_{1-x}Cd_xSnSe_4$ has two strong peaks at 173 and 196 cm^{-1} whose positions "did not change noticeably with x," and a less intense peak in the region of 231–253 cm^{-1}, depending on x (higher frequency corresponds to higher Cd concentration). Without discussing the intensities (as Raman scattering matrix elements are not included in our calculation), we note that the two candidates for the former peaks in our calculation are those at 174 and 187 cm^{-1}, both with noticeable Zn contribution but predominantly Cu-like. The outmost mode at 239 cm^{-1} has the strongest fraction of Zn vibration, and hence expected to be affected by the Zn concentration in the way the experiment suggests it. Moreover, the Raman spectrum in Fig. 3 of Ref. 33 shows a peak at about 80 cm^{-1}, in perfect agreement with our Cu-Zn-Sn "Raman-visible" modes of 75 and 81 cm^{-1}.

Turning now to the results for the stannite phase, we note that its phonons spectrum (Fig. 5, bottom panel) is somehow more deviant from that of $CuInSe_2$, although the frequency ranges occupied by distinct groups of lines remain the same. This difference comes down to the Cu-only/Zn+Sn plane-by-plane cationic sequence of stannite, in contrast to the Cu+Zn/Cu+Sn in kesterite, even as the local neighborhood of each anion is the same. To understand this importance, we note that the Cu-Se-Sn-Se-Cu and Cu-Se-Zn-Se-Cu chains, which transversed the kesterite structure in the $[\bar{1}10]$ and $[110]$ directions, give place in stannite to Cu-Se-Cu-Se-Cu and Zn-Se-Sn-Se-Zn ones; the "kesteritelike" chains can still be identified but they are no more planar and transverse the crystal in a fancy way. For an example of a relatively "invariant" vibration, let's have a closer look at the mode 17 of kesterite (Fig. 6) which is "longitudinal" with respect to one Cu-Se-Sn-Se-Cu chain (in the bottom part of the cube shown) and "transversal" with respect to the other chain (in the upper part of the cube). The Se anions are involved in the longitudinal motion and at rest relative to the transversal motion; the other partner (mode 16) of the same vibration line interchanges the roles of two chains. An astonishingly similar vibration pattern in stannite (mode 17 in Fig. 7) involves Zn, at place of Cu, at minutely smaller vibration frequency.

A remarkable difference between kesterite and stannite is revealed in the nature of Zn-related modes. In both systems, the upmost mode is essentially a Zn-against-Se vibration. However, in kesterite this is a longitudinal vibration within the Cu-Se-Zn-Se-Cu chains which are confined to (110), or $(1\bar{1}0)$, planes, and hence, for both Zn and Se, roughly occurs in the (x,y) plane. In stannite, the Cu-Se-Zn-Se-Cu chains

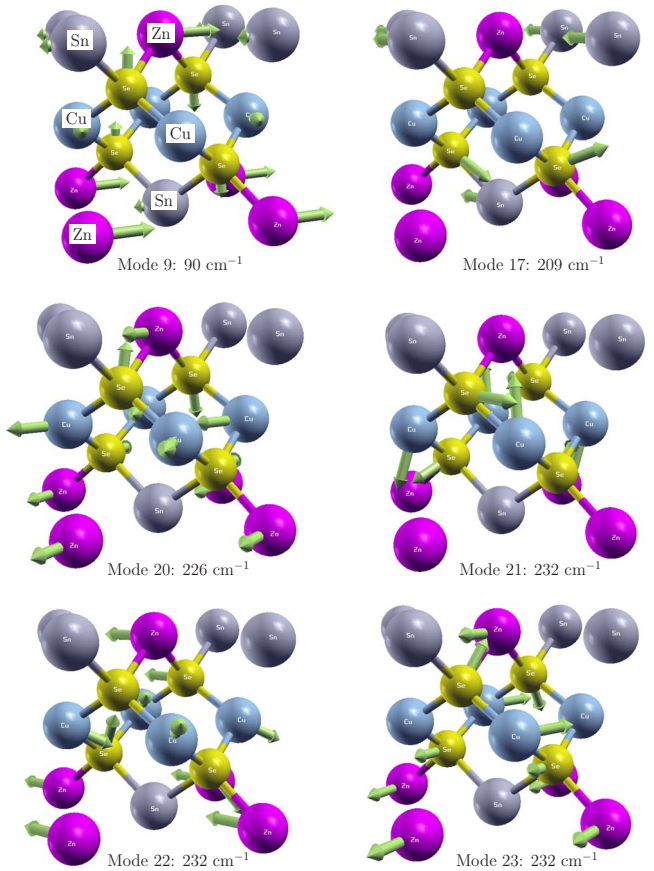

FIG. 7. (Color online) Vibration patterns in selected modes of CZTSe-stannite. See text for discussion.

can still be identified but they now run vertically throughout the crystal, having kinks and propelling in a helical manner, e.g., they are no more confined to any single plane. The resulting net z displacement of Zn (in the mode 24 of stannite) is a compromise from averaging longitudinal Zn movement in such chains while having only one Zn atom per unit cell. The four Se atoms vibrate in antiphase to zinc, each one roughly along the bond to its relative Zn neighbor. Due to a kinked nature of chains, the frequency of such longitudinal vibration is substantially elevated (254 cm^{-1} in stannite vs 239 cm^{-1} in kesterite). We suggest that this highest vibration mode, which is well separated from the previous modes and well detectable (as discussed above), may be useful as a kesterite vs stannite structure probe.

Interestingly, a similar upward frequency shift due to kinked chains works in the other direction, coming from stannite to kesterite, with respect to other Zn-related modes. Among the modes at 232 cm^{-1} in stannite responsible for the last-to-highest peak in the Zn-related density of modes (Fig. 5, bottom panel), notably mode 21 contains a clear pattern of Cu-Se-Cu-Se-Cu longitudinal vibrations (with remote Zn being accidentally in resonance). Since each Cu atom in the stannite phase belongs to two such chains (with Se either above, or below, the Cu-only plane), the resulting Cu motion is along $\pm z$ whereas the displacement of each Se is cleanly along the chain it belongs to. In kesterite, a similar vibration pattern, with respect to the Cu-Se-Cu-Se-Cu se-

quence, is seen in the mode 22 at 237 cm^{-1}, with the difference that the Cu-Se chain in question now transverses the crystal along the z direction, forming kinks. A slight frequency difference is an apparent manifestation of the cation-anion chain "hardening" due to the formation of such kinks.

With the two above observations taken together, one understands different shape of the Zn-related vibration modes density in the upper (from 210 cm^{-1} on) segment: in stannite, the hardest mode experiences an upward shift, resulting in two-peak structure (at 232 and 254 cm^{-1}) whereas in kesterite, the lower mode is upward shifted, merging the vibration lines into a single peak near 237 cm^{-1}.

V. CONCLUSION

Our calculation reveals expected similarities in the electronic structure of CZTSe kesterite with CZTS, or with stannite phase of CZTSe studied and explained in detail before. The LDA yields a small negative indirect gap, at variance with experiment but in apparent agreement with other calculations. The vibration spectrum, in our knowledge not calculated before, reveals features which can be traced back to CIS but remain "silent" (or, not zone-center) in this compound. On the contrary, the diversification of cations in kesterite into three species gives rise to additional modes which should become visible in experiment spectra. A comparison with calculated vibration spectrum of stannite underlines close similarities but also some noticeable differences with that of kesterite. We suggest that notably the differences might turn out useful for structural identification of these structurally close phases of CZTSe.

ACKNOWLEDGMENTS

We appreciate enlightening discussions with Susanne Siebentritt, notably introducing us to the thematics of the compound in question. The calculations have been done using computation resources of the PMMS at the Paul Verlaine University, Metz.

[1] J. Paier, R. Asahi, A. Nagoya, and G. Kresse, Phys. Rev. B **79**, 115126 (2009).
[2] K. Ito and T. Nakazawa, Jpn. J. Appl. Phys., Part 1 **27**, 2094 (1988).
[3] H. Katagiri, K. Saitoh, T. Washio, H. Shinohara, T. Kurumadani, and S. Miyajima, Sol. Energy Mater. Sol. Cells **65**, 141 (2001).
[4] H. Katagiri, N. Ishigaki, T. Ishida, and K. Saito, Jpn. J. Appl. Phys., Part 1 **40**, 500 (2001).
[5] J.-S. Seol, S.-Y. Lee, J.-C. Lee, H.-D. Nam, and K.-H. Kim, Sol. Energy Mater. Sol. Cells **75**, 155 (2003).
[6] H. Katagiri, Thin Solid Films **480-481**, 426 (2005).
[7] T. Kobayashi, K. Jimbo, K. Tsuchida, S. Shinoda, T. Oyanagi, and H. Katagiri, Jpn. J. Appl. Phys., Part 1 **44**, 783 (2005).
[8] Satoshi Nakamura, Tsuyoshi Maeda, and Takahiro Wada, Phys. Status Solidi C **6**, 1261 (2009).
[9] S. Chen, X. G. Gong, A. Walsh, and S.-H. Wei, Appl. Phys. Lett. **94**, 041903 (2009).
[10] S. Chen, X. G. Gong, A. Walsh, and S.-H. Wei, Phys. Rev. B **79**, 165211 (2009).
[11] H. Matsushita, T. Maeda, A. Katsui, and T. Takizawa, J. Cryst. Growth **208**, 416 (2000).
[12] R. A. Wibowo, E. S. Lee, B. Munir, and K. H. Kim, Phys. Status Solidi A **204**, 3373 (2007).
[13] G. Kresse and J. Furthmüller, Comput. Mater. Sci. **6**, 15 (1996).
[14] G. Suresh Babu, Y. B. Kishore Kumar, P. Uday Bhaskar, and V. Sundara Raja, Semicond. Sci. Technol. **23**, 085023 (2008).
[15] K. Hönes, E. Zscherpel, J. Scragg, and S. Siebentritt, Physica B **404**, 4949 (2009).
[16] H. Katagiri, K. Jimbo, S. Yamada, T. Kamimura, W. S. Maw, T. Fukano, T. Ito, and T. Motohiro, Appl. Phys. Express **1**, 041201 (2008).
[17] J. M. Raulot, C. Domain, and J. F. Guillemoles, J. Phys. Chem. Solids **66**, 2019 (2005).
[18] J. E. Jaffe and A. Zunger, Phys. Rev. B **28**, 5822 (1983).
[19] T. Maeda, T. Takeichi, and T. Wada, Phys. Status Solidi A **203**, 2634 (2006).
[20] S. C. Abrahams and J. L. Bernstein, J. Chem. Phys. **59**, 5415 (1973).
[21] S. Schorr, M. Tovar, H.-J. Hoebler, and H.-W. Schock, Thin Solid Films **517**, 2508 (2009).
[22] SIESTA homepage, http://www.icmab.es/siesta/
[23] P. Ordejón, E. Artacho, and J. M. Soler, Phys. Rev. B **53**, R10441 (1996).
[24] J. M. Soler, E. Artacho, J. D. Gale, A. García, J. Junquera, P. Ordejón, and D. Sánchez-Portal, J. Phys.: Condens. Matter **14**, 2745 (2002).
[25] J. Junquera, Ó. Paz, D. Sánchez-Portal, and E. Artacho, Phys. Rev. B **64**, 235111 (2001).
[26] E. Anglada, J. M. Soler, J. Junquera, and E. Artacho, Phys. Rev. B **66**, 205101 (2002).
[27] A. V. Postnikov and M. V. Yakushev, Thin Solid Films **451-452**, 141 (2004).
[28] M. Ichimura and Y. Nakashima, Jpn. J. Appl. Phys. **48**, 090202 (2009).
[29] H. Matsushita, T. Ichikawa, and A. Katsui, J. Mater. Sci. **40**, 2003 (2005).
[30] I. D. Olekseyuk, L. D. Gulay, I. V. Dydchak, L. V. Piskach, O. V. Parasyuk, and O. V. Marchuk, J. Alloys Compd. **340**, 141 (2002).
[31] J. Łażewski, K. Parlinski, B. Hennion, and R. Foure, J. Phys.: Condens. Matter **11**, 9665 (1999).
[32] A. V. Postnikov, O. Pagès, and J. Hugel, Phys. Rev. B **71**, 115206 (2005).
[33] M. Altosaar, J. Raudoja, K. Timmo, M. Danilson, M. Grossberg, J. Krustok, and E. Mellikov, Phys. Status Solidi A **205**, 167 (2008).